
Unsupervised Training of Convex Regularizers using Maximum Likelihood Estimation

Hong Ye Tan¹ Ziruo Cai² Marcelo Pereyra³ Subhadip Mukherjee⁴ Junqi Tang⁵ Carola-Bibiane Schönlieb¹

Abstract

Unsupervised learning is a training approach in the situation where ground truth data is unavailable, such as inverse imaging problems. We present an unsupervised Bayesian training approach to learning convex neural network regularizers using a fixed noisy dataset, based on a dual Markov chain estimation method. Compared to classical supervised adversarial regularization methods, where there is access to both clean images as well as unlimited to noisy copies, we demonstrate close performance on natural image Gaussian deconvolution and Poisson denoising tasks.

1. Introduction

Image processing is a classical example of high-dimensional inverse problems, with examples ranging from image denoising and deconvolution, to phase retrieval or computed tomography. This problem is usually formulated as the recovery of a signal $x \in \mathcal{X}$ from a noisy measurement $y = Ax + w \in \mathcal{Y}$, with forward operator $A : \mathcal{X} \rightarrow \mathcal{Y}$ and some noise w . A common trait of these problems is ill-posedness, where the solution of $Ax = y$ can have zero or infinitely many solutions. This necessitates the use of regularized reconstruction operators. A classical method of solving this is using variational regularization, combining a data fidelity term with priors such as wavelet priors or total variation priors (Xu & Osher, 2007; Rudin et al., 1992). Recently, various end-to-end approaches utilizing neural networks have pushed the state-of-the-art for imaging, at the cost of heavy data and computational burden. These include direct neural network approaches, as well as iterative plug-and-play priors (Zhang et al., 2021; Venkatakrishnan et al., 2013).

¹Department of Applied Mathematics and Theoretical Physics, University of Cambridge, U.K. ²Shanghai Jiao Tong University, China ³Heriot-Watt University, Edinburgh, Scotland ⁴Department of Electronics and Electrical Communication Engineering, Indian Institute of Technology, Kharagpur, India ⁵School of Mathematics, University of Birmingham, U.K..

Variational models. One way to define the reconstruction of a measurement y is as the solution of a minimization problem $\min_x f_y(Ax) + R_\lambda(x)$ (Benning & Burger, 2018). Here, $f_y : \mathcal{Y} \rightarrow \mathbb{R}$ is a data fidelity function measuring how well the reconstruction x fits the measurement $y \in \mathcal{Y}$, and $R_\lambda : \mathcal{X} \rightarrow \mathbb{R}$ is a regularization functional that promotes some regularity conditions on the solution. In the case of Gaussian denoising, $A = I$, the fidelity can be taken to be $f_y(x) = \|x - y\|^2/2$ and regularization $R_\lambda(x) = \lambda \|\nabla x\|_{1,\mathcal{X}}$. This is commonly known as the total variation (TV) regularized solution. One advantage of using a variational model is interpretability over a fully end-to-end method, as minimizers of convex functions satisfy various nice properties. As mentioned previously, R_λ can be hand-crafted to the task at hand.

Bayesian approaches. Another paradigm takes a more Bayesian approach, aiming to characterize the posterior distribution (density) of x conditioned on observing the noisy measurement y . Using Bayes' rule, this distribution can be broken down as $p(x|y) = \ell(y|x)\pi(x)/Z(y)$, where $\ell(y|x) = p_w(y - Ax)$ is the likelihood arising from the noise distribution of w , π is the prior density on x , and $Z(y)$ is a normalizing constant. One distinct advantage of the Bayesian approach is the option of uncertainty quantification rather than point estimation, given sufficient computational resources (Carioni et al., 2023). This is used in various imaging methods such as Wasserstein generative adversarial networks (Arjovsky et al., 2017), and Cycle-GANs (Zhu et al., 2017), which utilize optimal transport to flow from noisy to clean images with a learned prior. Since Bayesian approaches use the entire distribution, one distinct advantage over other training methods is that paired training examples (such as clean-noisy pairs) are often not needed.

The variational formulation can be formulated as a special case of the Bayesian formulation. Given the negative prior log-density $g(x)$ and negative log-likelihood $\ell(y|x) = f_y(x)$, the maximum a-posteriori estimator (MAP) $x_{\text{MAP}} = \arg \max_x p(x|y) \propto \exp(-f_y(x) - g(x))$ is the minimizer of $\min_x f_y(x) + g(x)$. The likelihood can thus be interpreted as a fidelity term, and the prior as regularization. Tweedie's identity states that for a prior density $p(x)$, and p_ϵ given by convolving p with a Gaussian kernel of variance ϵ , the optimal MMSE denoiser D_ϵ^* satisfies

$(D_\epsilon^* - I)(x) = \epsilon \nabla \log p_\epsilon^*(x)$ (Efron, 2011; Laumont et al., 2022). That is, the denoising step is in the direction of the posterior score. This is one result that draws the link between direct reconstruction and statistical sampling, and raises the question: can we interpret reconstruction operators as statistical objects?

Learned regularization. The regularization term in the variational regularization framework can be learned. Notable examples include adversarial regularization and network Tikhonov (Mukherjee et al., 2021; Lunz et al., 2018; Li et al., 2020). In the presence of clean and noisy training pairs, one method is to minimize some distance metric between the reconstructed noisy images and the clean image, with some regularization to enforce regularity on the learned regularizer such as Lipschitzness. Another theme aims to penalize noisy images and promote clean images by maximizing and minimizing the regularizing terms respectively. Using the structure of a fidelity and regularizer allows for a more explicit description of the final reconstruction, and can improve the performance of a learned denoiser when used in an unrolled scheme (Zhang et al., 2021). We note that it is possible to indirectly learn R_λ by instead learning mappings such as the proximal prox_{R_λ} or ∇R_λ , while still maintaining well-posedness of the variational formulation. For example, under certain Lipschitz conditions, denoisers can be interpreted as proximal operators of weakly convex functions, allowing for another degree of regularity (Hurault et al., 2022).

Unsupervised learning. Many end-to-end approaches require paired clean ground truths x and measurements y , which can be limiting in cases where ground truth data is unavailable or expensive, such as in medical imaging. Some unsupervised approaches such as Noise2Noise generate an unlimited number of noisy measurements, where averaging out the empirical risks with the noisy targets leads to an approximation of the empirical risks when training with clean targets (Lehtinen et al., 2018). We are instead concerned with the situation where we have a finite amount of noisy data, such as one-shot corruption of a clean dataset. One such approach is the deep image prior, in which the a neural network is fed a random input, and subsequently has its parameters optimized to recover a noisy measurement with early stopping (Ulyanov et al., 2018). This has shown remarkable performance without any supervised data, using only the implicit regularization of the neural network architecture.

Equivariant learning is another unsupervised framework that learns reconstruction functions from only compressed measurements (Chen et al., 2021; Tachella & Pereyra, 2023). The general idea is the set of plausible signals in \mathcal{X} are invariant to a certain group of transformations \mathcal{G} . By “rotating” the range of the adjoint operator, or constructing virtual op-

erators corresponding to invariances of the forward operator, the learned operator is able to learn reconstructions that are approximately equivariant to the transformations, mitigating problems arising from nontrivial nullspaces. Equivalently, EI can be interpreted as removing artifacts that are not invariant under transformations in \mathcal{G} .

Bayesian estimation of parameters. While the above methods deals with setting regularization parameters such that the reconstructions minimize some metric such as data fidelity or equivariance, a Bayesian approach allows for a statistical interpretation of these reconstructions. Vidal et al. (2020) proposes a method of estimating the optimal parameters for TV regularized denoising or hyperspectral unmixing for a single image using maximum marginal likelihood estimation, which can then be used for post-hoc reconstruction. The dual Markov chain approach jointly maximizes the prior as well as the posterior, after which the reconstruction is given by a MAP estimate. This work proposes a similar MCMC-based stochastic approximation scheme, applied with significantly more parameters when used to train a convex neural network regularization term, as well as a straightforward extension to many training images.

1.1. Contributions

In this work, we propose a method of training convex regularizers with the following goals in mind.

1. Training a regularizing prior using *only noisy data*. In particular, we do not assume the existence of multiple noisy copies of the data, such as in Noise2Noise schemes (Lehtinen et al., 2018).
2. Reasonable convergence of MCMC in high dimensions. We observe that the regularizers trained in the proposed unsupervised manner have a strong regularizing effect that has a reasonable performance gap from corresponding supervised training.

2. Unsupervised Empirical Bayes Parameter Estimation

Given a compact set Θ and a regularizer $g_\theta(x)$ with free parameters $\theta \in \Theta$, the empirical Bayesian model selection paradigm estimates the parameters directly from observed data y , such as the MLE (Vidal et al., 2020)

$$\theta^* = \arg \max_{\theta \in \Theta} \log p(y|\theta), \quad (1)$$

where $p(y|\theta)$ is the marginal likelihood given by marginalizing over data $p(y|\theta) = \int f_y(\tilde{x}) dp(\tilde{x}|\theta)$. Standard assumptions on the likelihood $f_y(\tilde{x})$ include the negative log-likelihood $-\log f_y(\tilde{x})$ being convex and \mathcal{C}^1 with L_y -Lipschitz gradient (in x). One method of maximizing the

marginal likelihood is by gradient ascent on θ , which requires knowledge of $\nabla_{\theta} \log p(y|\theta)$. In the following section, we demonstrate how to approximately compute this gradient using only noisy measurements y using a double MCMC approach.

Denote the normalizing constant as

$$Z(\theta) = \int \exp(-g_{\theta}(x)) dx. \quad (2)$$

Then $p(x|\theta) = \exp(-g_{\theta}(x))/Z(\theta)$ is the prior distribution. While the marginal likelihood $\theta \mapsto p(y|\theta)$ is intractable, under certain regularity assumptions, it can be replaced with a noisy estimate and decomposed in the following manner (Vidal et al., 2020, Prop. A.1):

$$\begin{aligned} \nabla_{\theta} \log p(y|\theta) &= \int p(\tilde{x}|y, \theta) \nabla_{\theta} \log p(\tilde{x}, y|\theta) d\tilde{x} \\ &= - \int \nabla_{\theta} g_{\theta}(\tilde{x}) p(\tilde{x}|y, \theta) d\tilde{x} - \nabla_{\theta} \log(Z(\theta)). \end{aligned} \quad (3)$$

Noticing that $\nabla_{\theta} Z(\theta) = - \int \nabla_{\theta} g_{\theta}(\tilde{x}) \exp(-g_{\theta}(\tilde{x})) d\tilde{x}$,

$$\begin{aligned} \nabla_{\theta} \log Z(\theta) &= (\nabla_{\theta} Z(\theta))/Z(\theta) \\ &= - \int \nabla_{\theta} g_{\theta}(\tilde{x}) p(\tilde{x}|\theta) d\tilde{x}. \end{aligned} \quad (4)$$

Putting Equation (3) and Equation (4) together, we have the following integral expression for the marginal likelihood:

$$\nabla_{\theta} \log p(y|\theta) = \mathbb{E}_{\tilde{x}|\theta}[\nabla_{\theta} g_{\theta}(\tilde{x})] - \mathbb{E}_{\tilde{x}|y, \theta}[\nabla_{\theta} g_{\theta}(\tilde{x})]. \quad (5)$$

Using this decomposition, we are able to use MCMC methods to estimate the prior and normalizing constant, allowing us perform a noisy gradient descent on θ using only noisy observations y (and access to the likelihood ℓ). In this work, we extend the setup of Vidal et al. 2020 in the following manner:

1. The prior distributions are loosened from being of the form $p(x|\theta) \propto \exp(-\theta^{\top} g(x))$, to the more general parameterized form $p(x|\theta) \propto \exp(-g_{\theta}(x))$ for some convex g_{θ} .
2. The dimensions of the parameter space Θ are increased from 1 to the order of 10^5 , the dimensionality of a small convex regularizer.

Given a trained regularizer g_{θ} , the maximum a-posteriori (MAP) estimate for y given data x is given by

$$x^* = \arg \min_x \{\ell(y|x) + g_{\theta}(x)\},$$

intrinsically linking the regularizer with the problem of sampling from the posterior $p(x|y) = \ell(y|x)p(x|\theta)/Z(\theta)$.

2.1. Jointly Sampling Prior and Posterior

To compute the gradient of the marginal likelihood, we need to evaluate the integrals given in Equations (3) and (4). In general, this needs to be done numerically, though properties such as positive homogeneity can make this easier (Vidal et al., 2020, Sec. 3.3). Observe that Equation (5) is a difference of expectations of $\nabla_{\theta} g_{\theta}(\tilde{x})$, over the prior $p(x|\theta)$ and posterior $p(x|y, \theta)$. First assume that both the likelihood $\ell(y|\theta)$ and regularizer g_{θ} are smooth (in x). Following the setup of Vidal et al. (2020), we construct two Markov chains based on the unadjusted Langevin algorithm (ULA) to approximate these expectations (Dalalyan, 2017; Durmus & Moulines, 2017). For step-size parameters $\gamma, \gamma' > 0$, the chains are given as follows, where Z_k, Z'_k are i.i.d. standard Gaussians with identity covariance matrix:

$$R_{\gamma, \theta} : X_{k+1} = X_k - \gamma \nabla_x (f_y + g_{\theta})(X_k) + \sqrt{2\gamma} Z_{k+1}; \quad (6a)$$

$$\bar{R}_{\gamma', \theta} : \bar{X}_{k+1} = \bar{X}_k - \gamma' \nabla_x g_{\theta}(\bar{X}_k) + \sqrt{2\gamma'} Z'_{k+1}. \quad (6b)$$

The above Markov kernels $R_{\gamma, \theta}$ and $\bar{R}_{\gamma', \theta}$ target the posterior $p(x|y, \theta) = p(x, y|\theta)/p(y|\theta)$ and the prior $p(x|\theta)$ respectively. This allows us to use Monte Carlo estimators in Equation (5), and approximate the marginal posterior gradient $\nabla_{\theta} \log p(y|\theta)$. We note that it is possible to lift the smoothness requirement on ℓ or g_{θ} by using a different Markov kernel such as the Moreau–Yosida unadjusted Langevin algorithm (MYULA, Durmus et al., 2018). With the approximate marginal posterior gradient, we can apply stochastic gradient descent on θ with step-sizes δ_n , yielding the stochastic approximation proximal gradient (SAPG–ULA) Algorithm 1, as presented in (Vidal et al., 2020).

Algorithm 1 SAPG–ULA

Require: Initial $\{\theta_0, X_0^0, \bar{X}_0^0\}$, $(\delta_n, m_n)_{n \in \mathbb{N}}$, Θ , MC step-size parameters γ, γ' , iterations N

- 1: **for** $n = 0$ to $N - 1$ **do**
 - 2: **if** $n > 0$ **then**
 - 3: Set $X_0^n = X_{m_n-1}^{n-1}$
 - 4: Set $\bar{X}_0^n = \bar{X}_{m_n-1}^{n-1}$
 - 5: **end if**
 - 6: **for** $k = 0$ to $m_n - 1$ **do**
 - 7: Sample $X_{k+1}^n \sim R_{\gamma, \theta_n}(X_k^n, \cdot)$
 - 8: Sample $\bar{X}_{k+1}^n \sim \bar{R}_{\gamma', \theta_n}(\bar{X}_k^n, \cdot)$
 - 9: **end for**
 - 10: Set $\theta_{n+1} = \Pi_{\Theta}[\theta_n + \frac{\delta_{n+1}}{m_n} \sum_{k=1}^{m_n} \{\nabla_{\theta} g_{\theta}(\bar{X}_k^n) - \nabla_{\theta} g_{\theta}(X_k^n)\}]$.
 - 11: **end for**
-

A projection Π_{Θ} onto the compact set Θ is imposed after each update of θ . The following result states that convergence is attained when the Markov chain updates and the

updates for g_θ happen in an alternating fashion. This is key to computational efficiency.

Theorem 2.1 (De Bortoli et al. 2019, Theorem 3, De Bortoli et al. 2020, Theorem 6). *A single sample is sufficient, i.e., $m_n = 1$ leads to convergence.*

2.2. Reflecting Markov Chains

While the chains (6) sample from (biased versions of) the target posterior and prior distributions in the case of unrestricted domains, this does not hold true the case of constrained sampling. Indeed, the natural domain for images requires that pixel values be non-negative. Negative pixels may cause problems in the case of Poisson imaging, where the likelihood is zero for negative measurements. Melidonis et al. (2022) consider modifying the chains to force the Markov chain samples to adhere to the non-negativity constraint by projecting or reflecting into the target domain. A minor modification of Equation (6) leads to the following reflected Markov chains, where the absolute value of a vector $|v|$ is to be taken componentwise:

$$R_{\gamma,\theta} : X_{k+1} = |X_k - \gamma \nabla_x (f_y + g_\theta)(X_k) + \sqrt{2\gamma} Z_{k+1}|; \quad (7a)$$

$$\bar{R}_{\gamma',\theta} : \bar{X}_{k+1} = |\bar{X}_k - \gamma' \nabla_x g_\theta(\bar{X}_k) + \sqrt{2\gamma'} Z'_{k+1}|. \quad (7b)$$

Denote $\iota_{\mathbb{R}_+^d}(x)$ as the indicator function with the set $C = \mathbb{R}_+^d$:

$$\iota_C(x) = \begin{cases} 0, & x \in C, \\ +\infty, & x \notin C. \end{cases}$$

Let $E_\theta(x) = f_y(x) + g_\theta(x) + \iota_{\mathbb{R}_+^d}(x)$. From the above reflections on the boundary of \mathbb{R}_+^d , the original target distribution $p(x|\theta)$ and $p(x|y, \theta)$ are truncated and modified into the following ones:

$$p(x|y, \theta) = \frac{e^{-E_\theta(x)}}{\int_{\mathbb{R}_+^d} e^{-E_\theta(\tilde{x})} d\tilde{x}}, \quad (8)$$

$$p(x|\theta) = \frac{e^{-(g_\theta(x) + \iota_{\mathbb{R}_+^d}(x))}}{\int_{\mathbb{R}_+^d} e^{-g_\theta(\tilde{x})} d\tilde{x}}. \quad (9)$$

The algorithm (7a), (7b) are the discrete counterparts of the reflected SDE on \mathbb{R}_+^d constructed in (Melidonis et al., 2022). It can be shown that under suitable assumptions, the reflected SDE admits a unique invariant measure on \mathbb{R}_+^d (Melidonis et al., 2022, Thm 3.4).

2.3. Mini-Batching

The setups given in Vidal et al. (2020); Melidonis et al. (2022) are limited to reconstructions for single images, as well as only one or two scalar parameters. However, we aim to train a neural network regularizing prior on a standard

image dataset such as STL-10. Since computing gradients of g_θ over all images in the dataset is computationally infeasible, mini-batching is necessary. In this section, we present a straightforward extension of the SAPG scheme to the batched case in Algorithm 2, by using multiple posterior Markov chains and changing when the prior Markov chains are updated. This has the upside of only having to store one mini-batch worth of gradients at any given time.

We note that this can be interpreted as multiple pairs of posterior and prior chains $\{X^{n,b}, \bar{X}^n\}_{b=1}^B$, where the posterior chains $X^{n,b}$ are updated according to $R_{\gamma,\theta}$, and the prior chain is updated according to $\bar{R}_{\gamma',\theta}$. Since the prior Markov kernel \bar{R} does not depend on the measured data, using only one chain is sufficient.

Algorithm 2 Batched Reflected SAPG-ULA

Require: Number of batches B , batched measurements $\{Y_b\}_{b=1}^B$, Initial $\{\theta_0, X_{0,b}^0, \bar{X}_0^0\}_{b=1}^B$, $(\delta_n, m_n)_{n \in \mathbb{N}}$, Θ , parameters γ, γ' , iterations N ,

```

1: for  $n = 0$  to  $N - 1$  do
2:   if  $n > 0$  then
3:     Set  $X_{0,b}^{n,b} = X_{m_n-1}^{n-1,b}$  for  $b \in [B]$ 
4:     Set  $\bar{X}_0^n = \bar{X}_{m_n-1}^{n-1}$ 
5:   end if
6:   for  $k = 0$  to  $m_n - 1$  do
7:     Sample  $\bar{X}_{k+1}^n \sim \bar{R}_{\gamma',\theta_n}(\bar{X}_k^n, \cdot)$ 
8:     for  $b = 1$  to  $B$  do
9:       Sample  $X_{k+1}^{n,b} \sim R_{\gamma,\theta_n}(X_k^{n,b}, \cdot; Y_b)$ 
10:    end for
11:   end for
12:   Set  $\theta_{n+1} = \Pi_\Theta[\theta_n$ 
      +  $\frac{\delta_{n+1}}{m_n} \sum_{b=1}^B \sum_{k=1}^{m_n} \{\nabla_\theta g_\theta(\bar{X}_k^n) - \nabla_\theta g_\theta(X_k^{n,b})\}]$ .
13: end for

```

3. Experiments

In the following experiments, we will compare the proposed unsupervised MLE method with the t -gradient-step supervised training method as detailed in (Goujon et al., 2022), where we keep the same architecture with roughly 15.5K parameters for consistency. The supervised training method involves performing gradient steps to minimize the variational functional induced by the convex regularizer, which is then trained to minimize the ℓ_1 distance between the reconstructed image and the ground truth. We compare this supervised adversarial training profile to our proposed unsupervised training, which does not require noise-free images.

Equivariant imaging poses another interesting baseline to compare against. We use the same setup as (Scanvic et al., 2023), which recently extends the EI framework using scale transforms, used in cases where the forward operator and

Training Regime	MAP	MMSE (2×10^4)	MMSE (1×10^5)
Gradient step	25.74 (10 step)	–	–
SAPG	25.19	25.09	25.10
WS-SAPG	25.25	25.05	25.06
EI	27.11	–	–
TV	24.75	–	–
DIP-UNet-Adam	25.50	–	–
DIP-CNN-Adam	24.67	–	–
DIP-UNet-GD	21.80	–	–
DIP-CNN-GD	24.50	–	–

Table 1. Table of PSNR (dB) of the convex ridge regularizer trained for Gaussian deconvolution. The initial PSNR of the corrupted image is 22.38dB. The MAP regularization parameter for the MLE is $\lambda = 0.6$. Averaged over 50 test images.

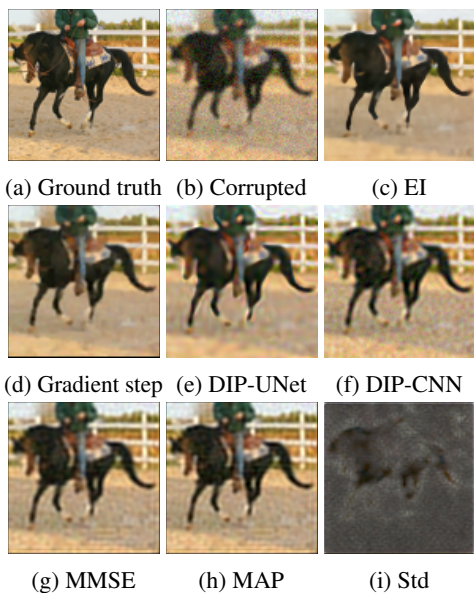


Figure 1. Visual comparison of various reconstructions of a noisy blurred test image. The unsupervised MAP and MMSE reconstructions of the proposed SAPG kernel contain visual artifacts compared to the adversarial training method. We observe that EI has the sharpest looking image, which is due to explicit knowledge of the forward operator as a blur kernel, as well as having a much richer end-to-end parameterization.

noise models are equivariant under the standard rotations and reflections. The learned reconstruction of the EI model takes the form of an end-to-end neural network, using the state-of-the-art SwinIR architecture, using 11.5M parameters (Liang et al., 2021). We train using the given parameters for up to 200 epochs, but use early stopping at 25 epochs due to divergence issues during training.

We additionally compare with the total variation prior $g(x) = \|\nabla x\|_1$ (Rudin et al., 1992), as well as using a deep image prior for reconstruction (Tachella et al., 2021; Ulyanov et al., 2018). For TV regularization, the regular-

ization parameter is chosen via a grid search to maximize PSNR with respect to the ground truth. For DIP, we compare using a U-Net as well as a convolutional neural network, optimized using Adam as in (Tachella et al., 2021). The reported PSNR is taken to be the highest with respect to the ground truth.

The regularizer architecture used for these experiments is the convex ridge regularizer (Goujon et al., 2022). This takes the form

$$R : \mathbf{x} \mapsto \sum_i \psi_i(\mathbf{w}_i^\top \mathbf{x}), \quad (10)$$

where $\psi_i : \mathbb{R} \rightarrow \mathbb{R}$ are convex profile functions (ridges), and $\mathbf{w}_i \in \mathbb{R}^d$ are learnable weights. The gradient of the regularizer can be expressed as

$$\nabla R(\mathbf{x}) = \mathbf{W}^\top \sigma(\mathbf{W}\mathbf{x}), \quad (11)$$

where $\mathbf{W} = [\mathbf{w}_1 \dots \mathbf{w}_p]^\top \in \mathbb{R}^{p \times d}$, and $\sigma : \mathbb{R}^p \rightarrow \mathbb{R}^p$ is a pointwise activation function with components $\sigma_i = \psi_i'$. Note that due to the convexity of ψ , the components σ_i are increasing. We use the same choice of architecture as (Goujon et al., 2022), where \mathbf{W} is modelled using a convolution.

To compute the MAP estimators of our trained regularizers, we minimize the negative log-posterior $\varphi(x) = \ell(y|x) + \lambda g_\theta(x)$, where ℓ is the negative log-likelihood (fidelity) function corresponding to the corruption operator, and g_θ is the learned convex regularizer. The regularization parameter λ is chosen via a grid search $\lambda \in \{0.1, 0.2, \dots, 1.0\}$. The negative log-posterior φ is minimized using the Adam optimizer for up to 10^4 iterations, with learning rate 10^{-3} and other parameters as default. We additionally consider the posterior mean after 2×10^4 and 1×10^5 iterations, labeled ‘MMSE’ in the figures and tables.

Training Regime	MAP	MMSE (2×10^4)	MMSE (1×10^5)
Gradient step	28.29 (10 step)	–	–
SAPG	27.94	26.65	27.52
WS-SAPG	28.14	27.34	27.75
EI	26.89	–	–
TV	24.09	–	–
DIP-UNet-Adam	26.50	–	–
DIP-CNN-Adam	26.28	–	–
DIP-UNet-GD	21.84	–	–
DIP-CNN-GD	26.59	–	–

Table 2. Table of PSNR (dB) of the convex ridge regularizer trained for Poisson denoising. We observe better performance of the learned priors compared to end-to-end reconstructions. The initial average PSNR of the corrupted images is 21.16dB. The MAP regularization parameter for the MLE is $\lambda = 0.6$. Averaged over 50 test images.

3.1. Gaussian Deconvolution

The first set of experiments is Gaussian deconvolution on the natural image dataset STL-10. The images consist of 96×96 color images, which are then corrupted with a Gaussian blur with kernel size 5 and blur strength 1, followed by additive 5% Gaussian noise. The negative log-likelihood is thus given by

$$f_y(x) = \frac{1}{2\sigma^2} \|Ax - y\|^2,$$

where A is the blur kernel. For SAPG, the step-sizes γ, γ' for the likelihood and prior Markov chains $R_{\gamma, \theta}, \bar{R}_{\gamma', \theta}$ respectively are given by $\gamma = \gamma' = 1e-4$.

We observe from Table 1 that the proposed unsupervised SAPG method is able to perform closely with the supervised t -gradient-step method, with a gap of only 0.5dB. Moreover, we observe that the MAP estimate with the learned reconstruction priors are generally better than the posterior mean estimates. The SAPG-learned prior also is competitive with/better than other priors such as TV or DIP, the latter of which still has a lack of theoretical properties. We are also able to plot the standard deviation of the Markov chain samples as seen in Figure 1i.

3.2. Poisson Denoising

Poisson denoising naturally arises in low-photon imaging, where the measurement takes integer pixel values. We can model the measurement using a Poisson random variable $y \sim \text{Pois}(\eta x)$ taken pixel-wise over an image space \mathbb{R}_{++}^n , where η is a parameter chosen such that the expected mean pixel intensity of y is a fixed mean intensity value (MIV). The forward operator is set to be the identity. In this case, the Poisson log-likelihood $y \sim \text{Pois}(\eta x)$ is given by

$$f_y(x) = \sum_{i \in [n]} [(\eta x)_i - y_i \log(\eta x_i) + \log(y_i!)] + \iota_{\mathbb{R}_{++}^n}(x),$$

$$f_y(x) = \eta \mathbf{1}_{\mathcal{I}} - y/x,$$

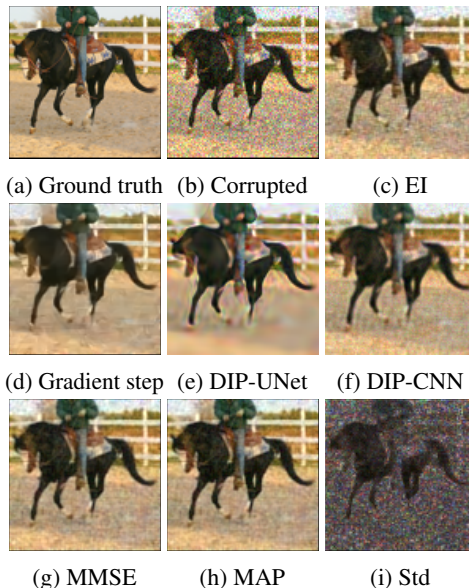


Figure 2. Visual comparison of reconstructions for Poisson denoising. SAPG, as shown in subfigures (g) and (h) both show significant denoising, but with the presence of artifacts. DIP has a strong smoothing effect, but also induces strange visual artifacts around the target as shown in subfigure (e).

where $\iota_{\mathbb{R}_{++}^n}(x)$ is 0 when all x_i are positive and $+\infty$ otherwise, and division of images is to be taken pixel-wise. The Poisson log-likelihood does not have a globally Lipschitz gradient, which makes this problem difficult compared to the Gaussian case due to requiring both approximating the log-likelihood as well as needing a small step-size. Therefore, we use the following modified log-likelihood given as follows for $b > 0$ (Melidonis et al., 2022),

$$\ell(y|x) = \sum_{i \in [n]} [\eta(x_i + b) - y_i \log(\eta(x_i + b)) + \log(y_i!)],$$

$$\nabla_x \ell(y|x) = \eta \mathbf{1}_{\mathcal{I}} - y/(x + b).$$

Training Regime	MAP	MMSE (2×10^4)	MMSE (1×10^5)
Gradient step	23.90 (10 step)	–	–
SAPG	23.73	23.62	23.55
WS-SAPG	23.79	22.81	23.05
EI	21.37	–	–
TV	22.20	–	–

Table 3. Table of PSNR (dB) of the convex ridge regularizer trained for Gaussian deconvolution, applied to uniform deconvolution. We observe significantly better transfer properties of the learned regularizers compared to the end-to-end EI schemes, with only a small drop in performance between the supervised and unsupervised versions. The initial PSNR of the corrupted image is 20.13dB. The MAP regularization parameter for the MLE is $\lambda = 0.7$. Averaged over 50 test images.

The introduction of $b > 0$ pushes the likelihood away from 0 and makes $\nabla_x \ell$ Lipschitz on \mathbb{R}_{++}^n . We use the parameter $b = \text{MIV}/100$ as suggested in (Melidonis et al., 2022). The mean intensity value is set to be $\lambda_{\text{MIV}} = 25$ for light Poisson denoising. For SAPG, the step-sizes for the likelihood and prior Markov chains are given by $\gamma = 5e-6$, $\gamma' = 1e-5$ respectively.

Table 2 compares the regularizer trained using the proposed unsupervised method, compared to that trained using t -gradient-step training. We again observe a reasonable gap of 0.15dB between our unsupervised method and the supervised method, using the same architecture. For this problem, we are also superior to equivariant imaging, as well as other image priors such as TV and DIP. This highlights the difficulty of Poisson denoising for end-to-end models, as observed previously due to the high Lipschitz constants and large data range.

3.3. Transfer to different forward operator

In addition to the Gaussian deconvolution experiments, we consider robustness of the learned model with respect to changes in forward operator. We evaluate the trained models on a 5×5 uniform blur kernel with the same additive 5% Gaussian noise.

Table 3 shows the reconstruction results for transferring the learned models between different tasks. We observe a significantly larger drop in performance from the EI model, which is trained on a specific forward operator, which introduces more blur artifacts. On the other hand, the model-based gradient step reconstruction still produces reasonably good results. The unsupervised versions have similar performance, albeit with added visual artifacts. This may be due to image prior components that are difficult to learn from only noisy patches.

4. Conclusion

We proposed an unsupervised method of training a convex neural network based image prior based on the stochastic

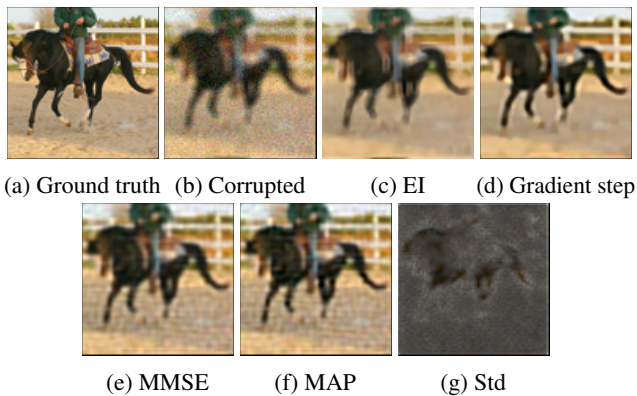


Figure 3. Visual comparison of reconstructions for uniform deconvolution when using models trained for Gaussian deconvolution. We observe more residual blur for EI when compared to the model-based prior in the bottom row.

approximate proximal gradient algorithm, that works only single copies of corrupted data. Prior works consider a family of total variation priors, here we consider a parameterization with significantly more parameters. Experiments demonstrate that the proposed method produces priors that are near competitive when compared to the alternative supervised training method for various image corruption operators, maintaining significantly better generalization properties when compared to end-to-end methods. Moreover, we present convergence theory for the proposed Markov chains, demonstrating convergence in the more general case of a non-convex image prior architecture.

Interesting future works could include a convergence analysis in the discrete case or with accelerated versions of the training algorithm such as Adam instead of SGD, or SK-ROCK instead of ULA.

References

- Arjovsky, M., Chintala, S., and Bottou, L. Wasserstein generative adversarial networks. In *International conference on machine learning*, pp. 214–223. PMLR, 2017.
- Benning, M. and Burger, M. Modern regularization methods for inverse problems. *Acta numerica*, 27:1–111, 2018.
- Carioni, M., Mukherjee, S., Tan, H. Y., and Tang, J. Unsupervised approaches based on optimal transport and convex analysis for inverse problems in imaging. *arXiv preprint arXiv:2311.08972*, 2023.
- Chen, D., Tachella, J., and Davies, M. E. Equivariant imaging: Learning beyond the range space. In *Proceedings of the IEEE/CVF International Conference on Computer Vision*, pp. 4379–4388, 2021.
- Dalalyan, A. S. Theoretical guarantees for approximate sampling from smooth and log-concave densities. *Journal of the Royal Statistical Society Series B: Statistical Methodology*, 79(3):651–676, 2017.
- De Bortoli, V., Durmus, A., Pereyra, M., and Vidal, A. F. Efficient stochastic optimisation by unadjusted Langevin Monte Carlo. application to maximum marginal likelihood and empirical Bayesian estimation. *arXiv preprint arXiv:1906.12281*, 2019.
- De Bortoli, V., Durmus, A., Pereyra, M., and Vidal, A. F. Maximum likelihood estimation of regularization parameters in high-dimensional inverse problems: an empirical bayesian approach. part ii: Theoretical analysis. *SIAM Journal on Imaging Sciences*, 13(4):1990–2028, 2020.
- Durmus, A. and Moulines, E. Nonasymptotic convergence analysis for the unadjusted langevin algorithm. *The Annals of Applied Probability*, 27(3):1551–1587, 2017.
- Durmus, A., Moulines, E., and Pereyra, M. Efficient bayesian computation by proximal markov chain monte carlo: when langevin meets moreau. *SIAM Journal on Imaging Sciences*, 11(1):473–506, 2018.
- Efron, B. Tweedie’s formula and selection bias. *Journal of the American Statistical Association*, 106(496):1602, 2011.
- Goujon, A., Neumayer, S., Bohra, P., Ducotterd, S., and Unser, M. A neural-network-based convex regularizer for image reconstruction. *arXiv preprint arXiv:2211.12461*, 2022.
- Hurault, S., Leclaire, A., and Papadakis, N. Proximal denoiser for convergent plug-and-play optimization with nonconvex regularization. In *International Conference on Machine Learning*, pp. 9483–9505. PMLR, 2022.
- Laumont, R., Bortoli, V. D., Almansa, A., Delon, J., Durmus, A., and Pereyra, M. Bayesian imaging using plug & play priors: when langevin meets tweedie. *SIAM Journal on Imaging Sciences*, 15(2):701–737, 2022.
- Lehtinen, J., Munkberg, J., Hasselgren, J., Laine, S., Karras, T., Aittala, M., and Aila, T. Noise2noise: Learning image restoration without clean data. In *International Conference on Machine Learning*, pp. 2965–2974. PMLR, 2018.
- Li, H., Schwab, J., Antholzer, S., and Haltmeier, M. Nett: Solving inverse problems with deep neural networks. *Inverse Problems*, 36(6):065005, 2020.
- Liang, J., Cao, J., Sun, G., Zhang, K., Van Gool, L., and Timofte, R. Swinir: Image restoration using swin transformer. In *Proceedings of the IEEE/CVF international conference on computer vision*, pp. 1833–1844, 2021.
- Lunz, S., Öktem, O., and Schönlieb, C.-B. Adversarial regularizers in inverse problems. *Advances in neural information processing systems*, 31, 2018.
- Melidonis, S., Dobson, P., Altmann, Y., Pereyra, M., and Zygalakis, K. C. Efficient Bayesian computation for low-photon imaging problems. *arXiv preprint arXiv:2206.05350*, 2022.
- Mukherjee, S., Carioni, M., Öktem, O., and Schönlieb, C.-B. End-to-end reconstruction meets data-driven regularization for inverse problems. *Advances in Neural Information Processing Systems*, 34:21413–21425, 2021.
- Rudin, L. I., Osher, S., and Fatemi, E. Nonlinear total variation based noise removal algorithms. *Physica D: nonlinear phenomena*, 60(1-4):259–268, 1992.
- Scanvic, J., Davies, M., Abry, P., and Tachella, J. Self-supervised learning for image super-resolution and deblurring. *arXiv preprint arXiv:2312.11232*, 2023.
- Tachella, J. and Pereyra, M. Equivariant bootstrapping for uncertainty quantification in imaging inverse problems. *arXiv preprint arXiv:2310.11838*, 2023.
- Tachella, J., Tang, J., and Davies, M. The neural tangent link between cnn denoisers and non-local filters. In *Proceedings of the IEEE/CVF Conference on Computer Vision and Pattern Recognition*, pp. 8618–8627, 2021.
- Ulyanov, D., Vedaldi, A., and Lempitsky, V. Deep image prior. In *Proceedings of the IEEE conference on computer vision and pattern recognition*, pp. 9446–9454, 2018.
- Venkatakrishnan, S. V., Bouman, C. A., and Wohlberg, B. Plug-and-play priors for model based reconstruction. In *2013 IEEE global conference on signal and information processing*, pp. 945–948. IEEE, 2013.

- Vidal, A. F., De Bortoli, V., Pereyra, M., and Durmus, A. Maximum likelihood estimation of regularization parameters in high-dimensional inverse problems: An empirical bayesian approach part i: Methodology and experiments. *SIAM Journal on Imaging Sciences*, 13(4):1945–1989, 2020.
- Xu, J. and Osher, S. Iterative regularization and nonlinear inverse scale space applied to wavelet-based denoising. *IEEE Transactions on Image Processing*, 16(2):534–544, 2007.
- Zhang, K., Li, Y., Zuo, W., Zhang, L., Van Gool, L., and Timofte, R. Plug-and-play image restoration with deep denoiser prior. *IEEE Transactions on Pattern Analysis and Machine Intelligence*, 44(10):6360–6376, 2021.
- Zhu, J.-Y., Park, T., Isola, P., and Efros, A. A. Unpaired image-to-image translation using cycle-consistent adversarial networks. In *Proceedings of the IEEE international conference on computer vision*, pp. 2223–2232, 2017.